Naval Research Laboratory

Washington, DC 20375-5000

NRL Report 9144

Reflection Driven Ship Wake Contrasts in the Infrared

I. B. SCHWARTZ AND R. G. PRIEST

Advanced Concepts Branch
Optical Sciences Division

August 23, 1988

SECURITY CLASSIFICATION OF THIS PAGE

REPORT DOCUMENTATION PAGE

Form Approved
OMB No 0704-0188

1a REPORT SECURITY CLASSIFICATION UNCLASSIFIED	1b RESTRICTIVE MARKINGS
2a SECURITY CLASSIFICATION AUTHORITY	3 DISTRIBUTION / AVAILABILITY OF REPORT Approved for public release: distribution unlimited.
2b DECLASSIFICATION / DOWNGRADING SCHEDULE	
4 PERFORMING ORGANIZATION REPORT NUMBER(S) NRL Report 9144	5 MONITORING ORGANIZATION REPORT NUMBER(S)
6a NAME OF PERFORMING ORGANIZATION Naval Research Laboratory 6b OFFICE SYMBOL (If applicable) Code 6520	7a NAME OF MONITORING ORGANIZATION
6c ADDRESS (City, State, and ZIP Code) Washington, DC 20375-5000	7b ADDRESS (City, State, and ZIP Code)
8a NAME OF FUNDING / SPONSORING ORGANIZATION U.S. Air Force 8b OFFICE SYMBOL (If applicable)	9 PROCUREMENT INSTRUMENT IDENTIFICATION NUMBER
8c ADDRESS (City, State, and ZIP Code) Los Angeles, CA 90009-2960	10 SOURCE OF FUNDING NUMBERS PROGRAM ELEMENT NO: 63224C PROJECT NO: (SDI) TASK NO: WORK UNIT ACCESSION NO: EX-158-076

11 TITLE (Include Security Classification)
Reflection Driven Ship Wake Contrasts in the Infrared

12 PERSONAL AUTHOR(S)
Schwartz, I.B. and Priest, R.G.

13a TYPE OF REPORT	13b TIME COVERED	14 DATE OF REPORT (Year, Month, Day)	15 PAGE COUNT
Interim	FROM 10/87 TO 10/88	1988 August 23	20

16 SUPPLEMENTARY NOTATION

17 COSATI CODES			18 SUBJECT TERMS (Continue on reverse if necessary and identify by block number)
FIELD	GROUP	SUB-GROUP	Ship wakes, Rough surface, Infrared

19 ABSTRACT (Continue on reverse if necessary and identify by block number)

Contrast between a ship's wake and a rough sea is considered from a probabilistic approach. A probability slope model of a rough sea is given in terms of the fraction of facets that reflect and emit infrared radiation into a sensor. It is shown computationally that the rough sea, when viewed near grazing, can appear much cooler than a smooth sea. Furthermore, the expected contrast between a ship's wake and its background can be driven by a reflection phenomenon rather than by a real temperature difference. Also, it is shown that the apparent temperature of a wake can be warmer than its background even though the intrinsic temperatures of the wake and background are the same. The rough sea background model takes into account self-shadowing of the sea surface that is important when the sea is viewed at near grazing angles.

20 DISTRIBUTION / AVAILABILITY OF ABSTRACT	21 ABSTRACT SECURITY CLASSIFICATION
☒ UNCLASSIFIED/UNLIMITED ☐ SAME AS RPT ☐ DTIC USERS	UNCLASSIFIED
22a NAME OF RESPONSIBLE INDIVIDUAL Ira B. Schwartz	22b TELEPHONE (Include Area Code) (202) 767-1361 22c OFFICE SYMBOL Code 6522

DD Form 1473, JUN 86 *Previous editions are obsolete.* SECURITY CLASSIFICATION OF THIS PAGE

S/N 0102-LF-014-6603

CONTENTS

1. INTRODUCTION 1

2. STATISTICS OF FACET PROJECTED AREAS 2

3. EMISSIVITY AND REFLECTIVITY 4

4. ROUGH SEA RADIANCE 5

5. APPLICATION TO SHIP WAKES 6

6. DISCUSSION 12

REFERENCES 13

APPENDIX A — Derivation of Slope Probability Density 15

REFLECTION DRIVEN SHIP WAKE CONTRASTS IN THE INFRARED

1. INTRODUCTION

The infrared signature of ships and their wakes is most often described in terms of contrast to the background infrared signature of the sea. Since the contrast signature of ships and their wakes involves the signature of the rough sea, an important task for signature modeling is to calculate the radiance of the sea surface as a function of viewing angle. The complication in the modeling arises because of the background, which is a rough sea surface. Wakes, on the other hand, appear as smoother surfaces. Since the infrared wavelength is much shorter than the length scale of disturbances on the water's surface, the rough sea may be thought of as an ensemble of small facets, each of which emits and reflects infrared radiation. Facets can reflect radiation from the sky and from other facets. In cases where the length (corresponding to the projection of the instantaneous field of view (IFOV)) of the sensor onto the ocean surface is greater than the length scale of sea disturbances, reflection and emission properties may be calculated by averaging over facets weighted by the probability density function for facet orientation.

The distribution of facet orientations can have a significant effect on the infrared radiation emanating from the sea surface. If the sea were smooth and flat, all the facets would be horizontally oriented. However when a rough sea surface is viewed near grazing, most of the facets seen by the sensor are tipped away from the horizontal toward the sensor [Goodell 1971, Menat 1976]. This phenomenon impacts upon both the amount of radiation emitted from the sea and the amount of radiation reflected from the sky. The average tilt angle causes radiation from elevation angles relatively higher in the sky to be reflected as would be the case if the sea where not rough. Since the strength of sky radiation decreases with increasing elevation angle, the effect of sea roughness is to decrease the amount of radiation reflected from the sky. At the same time, the decreased angle of incidence to the facet increases the emissivity of the facet [Schwartz and Hon 1986], which increases the amount of radiation emitted from the facet. At angles very near grazing, the reflected radiation decrease is larger than the emitted radiation increase. For other angles, the situation is reversed.

A major theoretical problem is that some facets are hidden from view by others. This is called the hidden surface problem, or shadowing problem. Two approaches to this statistical problem are possible. The first approach is to calculate the bidirectional reflectance distribution function (BRDF) under the assumption that there is no shadowing and then to introduce some heuristic corrections to take shadowing into account. This approach has been studied by Torrance and Sparrow [1967] for the case of rough material surfaces and by Maxwell et al. [1973] for the case of rough water. The second approach is to calculate the contribution to the total surface area seen by a sensor made by facets of a given orientation. This approach permits a simple adjustment to one of the effects of shadowing. The second approach is presented in this report. Both approaches lead to the same result in cases where there is no shadowing. We show that the simple correction allowed by the second approach leads to reasonable results for viewing angles near grazing incidence.

Manuscript approved April 18, 1988.

Section 2 presents the statistics needed to generate the facet distribution, and a simple model is shown to account for shadowing. The orientation of each facet affects the emissivity and reflectivity since both have angular dependence. Section 3 shows the relevant geometry and how facet reflectivity and emissivity depend on facet orientation. By using these results, Section 4 describes how the apparent radiance of the rough sea compares with that of a smooth sea. Finally, Section 5 presents the application to the problem of ship wakes. This section describes the conditions under which a ship's wake may appear to have a temperature that is warmer than its background.

2. STATISTICS OF FACET PROJECTED AREAS

Here we calculate the waveslope probability density function. An analytic result is available for the case where the wave amplitudes are sufficiently small that linear superposition of amplitudes is valid. The essential elements of this calculation have appeared in the literature [Beckmann and Spizzichino 1963]. (For completeness, the derivation is presented in Appendix A.) The central result can be expressed in terms of a probability density for the orientation of a unit vector $\hat{n}$ normal to the surface of a facet. The simplest description of this density is in terms of a system of spherical polar coordinates with the polar axis (the z axis) in the zenith direction and azimuth measured with respect to the upwind direction (the x axis). If θ and ϕ are (respectively) the polar and the azimuthal angles of $\hat{n}$, the probability density is:

$$p(\theta,\phi) = (1/2\pi)\,(ab)^{-1} \tan\theta \sec^2\theta\, e^{-\tan^2\theta A(\phi)}, \tag{1}$$

with

$$A(\phi) = \frac{1}{2}\left[\frac{\cos^2\phi}{a^2} + \frac{\sin^2\phi}{b^2}\right],$$

where a^2 is the variance of the derivative of the waveslope in the upwind direction and b^2 is the variance in the crosswind direction. Equation (1) may be thought of as the angular probability density for finding the facet at a given place on the surface, oriented such that its normal has the angular coordinates θ,ϕ. We assume there is no correlation between upwind and crosswind directions.

The basis of the approach developed in this report is the calculation of a fraction of the total projected area $f(\theta,\phi)$ seen by a sensor. This is the fraction contributed by facets falling in an infinitesimal angular range center at θ,ϕ. Once this fraction is determined, it can be used to weight the reflection and emission contributions of the facets to the net observed radiance. We define two types of projected areas. The first type is the horizontally projected area, which is obtained by projecting a facet or group of facets onto the horizontal plane. The second is the line-of-sight (LOS) projected area. LOS projected area is obtained by projecting a facet or group of facets onto a plane normal to a vector parallel to the LOS to the sensor. The probability density function $p(\theta,\phi)$ is related to the horizontally projected area in the following way: the horizontally projected area ΔA_h contributed by facets with orientations in the infinitesimal angular range $\Delta\theta\Delta\phi$ centered at θ,ϕ is given by:

$$\Delta A_h = A_h p(\theta,\phi)\Delta\theta\Delta\phi, \tag{2}$$

where A_h is the total horizontally projected area in the region under consideration. The unprojected surface area ΔA of the same group of facets is $\Delta A_h/\cos(\theta)$. That ΔA is greater than ΔA_h is a reflection of the well-known fact that the total surface area of a rough surface is greater than the horizontal

area that it covers. The LOS projected area of this same group of facets ΔA_{LOS} is given by $\Delta A \cos(\Omega)$, where Ω is the angle between the normal to the facet and the LOS from the facet to the sensor. The expression for ΔA_{LOS} in terms of the probability density function is thus:

$$\Delta A_{LOS} = A_h p(\theta,\phi) \frac{\cos(\Omega)}{\cos(\theta)} \Delta\theta\Delta\phi. \tag{3}$$

The total LOS projected area can be obtained by integrating the right-hand side (RHS) of Eq. (3) with respect to (θ,ϕ) over the upper hemisphere.

Notice that while θ is constrained to lie between 0 and $\pi/2$ there is no similar constraint on Ω. Consequently the RHS of Eq. (3) can be negative for some orientations of the LOS to the sensor. Equation (3) associates negative projected areas with facets that are oriented such that their normal vector points away from the sensor. When the RHS of Eq. (3) is integrated, the negative projected areas contributed by facets that point away from the sensor partially cancel the positive projected areas of other facets. The correct contribution for these facets is 0, since they face away from the sensor. (The model considered here does not take multiple reflections into account.) We modify Eq. (3) by multiplying by $H(\pi/2 - \Omega)$, where $H(x)$ is 1 when $x > 0$, and zero otherwise:

$$\Delta A_{LOS} = A_h p(\theta,\phi) \frac{\cos(\Omega)}{\cos(\theta)} H(\pi/2 - \Omega). \tag{4}$$

The preceding projected area discussion makes it possible to give an expression for the fractional projected area $\hat{f}(\theta,\phi)$. The quantity $\hat{f}(\theta,\phi)\Delta\theta\Delta\phi$ is defined to the fraction of the LOS projected area seen by the sensor that is contributed by facets with orientations in the range $\Delta\theta\Delta\phi$ centered at θ,ϕ. It is given by

$$f(\theta,\phi) = \frac{p(\theta,\phi) \frac{\cos(\Omega)}{\cos(\theta)} H(\pi/2 - \Omega)}{\int p(\theta,\phi) \frac{\cos(\Omega)}{\cos(\theta)} H(\pi/2 - \Omega) d\theta d\phi}. \tag{5}$$

That is, $f(\theta,\phi)$ is the expression of Eq. (3) is divided by the whole projected area seen by the sensor. The limits of the integration here and throughout this report are understood to be 0 to 2π for the azimuthal angles, and 0 to $\pi/2$ for the polar angles.

An alternative method for arriving at Eq. (5) involves consideration of a shadowing factor. This is the probability that a facet of given orientation is not hidden from view of the sensor. This problem has been analyzed in the context of radar detection [Smith 1967]. Ignoring correlation of waveheight and slope, the result is that the shadowing factor is proportional to $H(\pi/2 - \Omega)$. The proportionality factor is independent of facet orientation. The step from Eq. (4) to Eq. (5) can be viewed as the replacement of LOS projected areas with the product of LOS projected area and the appropriate shadowing factor.

The central idea introduced here is to use the expression of Eq. (5) to weight facet contributions to the net radiance. For comparison with the results of the BRDF approach, notice that the integral in the denominator of Eq. (5) can be explicitly carried out in the nonshadowing case. In this case, the function H is identically equal to unity. Elementary trigonometry may be used to express $\cos(\Omega)$ in terms of (θ,ϕ) and $(\hat{\theta},\hat{\phi})$:

$$\cos(\Omega) = \cos(\theta)\cos(\hat{\theta}) + \sin(\theta)\sin(\hat{\theta})\cos(\phi - \hat{\phi}), \tag{6}$$

where $\hat{\theta}$ and $\hat{\phi}$ are the polar and azimuthal angles of a unit vector $\hat{r}$ that is parallel to the LOS to the sensor. (See Fig. 1 for the coordinate system specification.) The integral in the denominator of Eq. (5) thus involves two terms. The first term evaluates immediately to cos $(\hat{\theta})$ because the probability density is normalized. The second term involves the integral of the product of cos $(\phi - \hat{\phi})$ and $p(\theta,\phi)$. The probability functions considered here have inversion symmetry, i.e., $p(\theta,\phi) = p(\theta,\pi - \phi)$. With this condition, it is easy to see that the second integral is 0. However it can be shown that this integral vanishes under more general conditions. The integral in the denominator of Eq. (5) thus evaluates to cos $(\hat{\theta})$ in the nonshadowing case. Thus in this case:

$$\hat{f}(\theta,\phi) = p(\theta,\phi) \frac{\cos(\Omega)}{\cos(\theta)\cos(\hat{\theta})}. \tag{7}$$

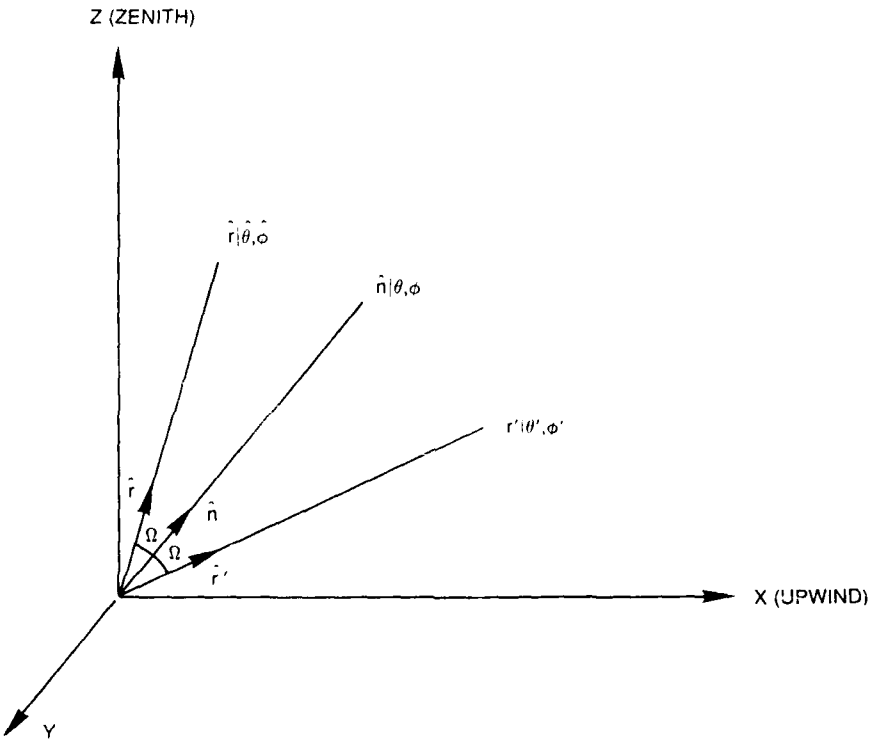

Fig. 1 — Local coordinate system for a facet. $\hat{r}$ is the unit view vector, r' is the reflected unit vector from the sky, and n is the unit normal to the facet.

3. EMISSIVITY AND REFLECTIVITY

The facet emissivity ϵ and reflectivity ρ are both functions of the angle Ω. The Fresnel formula for unpolarized radiation may be used to calculate $\rho(\Omega)$ if the complex optical constant for water is specified. The appropriate value is obtained by computing an average weighted by the response function of the sensor. Kirchhoff's law in the form $\epsilon = 1 - \rho$ may be used to obtain the angularly dependent emissivity. The intrinsic radiance R_i is given by $R_i = \epsilon(\Omega)R_B$, where R_B is the radiance of a blackbody at sea temperature. The reflected radiance R_r is given by $R_r = \rho(\Omega)R_s(\theta')$, where R_s is the sky radiance. The sky radiance depends on the angle θ' between the unit vector $\hat{r}$ and the zenith direction. The unit vector $\hat{r}$ is parallel to the ray generated by the reflection of the LOS from the

sensor by the facet. It has the angular coordinates θ',ϕ'. A vector expression can be given for $\hat{r}$ in terms of $\hat{n}$ and $\hat{r}$:

$$\hat{r}' = 2\cos(\Omega)\hat{n} - \hat{r}. \tag{8}$$

An expression for θ' in terms of Ω and θ,ϕ is obtained from this equation by taking the inner product of both sides of the equation with the unit vector pointing in the zenith direction.

$$\cos(\theta') = 2\cos(\Omega)\cos(\theta) - \cos(\hat{\theta}). \tag{9}$$

4. ROUGH SEA RADIANCE

The apparent radiance of the rough sea R_a is the expected value of the sums of R_i and R_r. This expected value is given by:

$$R_a(\hat{\theta}) = \int_0^{\pi/2} d\theta \int_0^{2\pi} d\phi \hat{f}(\theta,\phi)\{[1 - \rho(\Omega)]R_B + \rho(\Omega)R_s(\theta')\}. \tag{10}$$

Here the form of $\hat{f}$ is given by Eqs. (5) and (1), Ω is given by Eq. (6), and θ' is given by Eq. (9). The Fresnel formula is to be used for $\rho(\Omega)$, and the function R_s must be specified. An atmospheric modeling code such as Lowtran VI can be used to create a tabulated form of this function. Since $\hat{f}$ is a normalized weighting function, it can be verified that Eq. (10) satisfies a consistency relation. Specifically, in the case where R_s is a constant equal to R_B, one finds that $R_a = R_B$. This result is required by the second law of thermodynamics.

As mentioned in Section 1, the results obtained here agree with those obtained by using the BRDF approach when there is no shadowing. In this case, $\hat{f}$ is given by Eq. (7). If this form is substituted into Eq. (10) with the $p(\theta,\phi)$ given by Eq. (1) with $a^2 = b^2 = \sigma^2$ (isotropic case), the weighting terms in Eq. (10) become:

$$\frac{\tan(\theta)\cos(\Omega)\exp(-\tan^2(\theta)/\sigma^2)}{\cos^3(\theta)\cos(\hat{\theta})}. \tag{11}$$

Apart from notational differences, this weighting factor is the same as the one in Lecompte [1973].

To see the typical magnitude of the effects caused by a rough sea, a function R_s must be chosen. As an example, we have exercised the Lowtran program with summer midlatitude parameters and have obtained the long wave infrared (IR) (8 to 12 μm) sky radiance form, Fig. 2. For convenience, the value of the blackbody radiance of the sea R_B that appears in Eq. (10) was taken to be equal to the value of R_s at the horizon. This corresponds to selecting temperatures of the sea and of the air just above the sea to be equal. These Lowtran results, together with Eq. (10) (with $a^2 = b^2 = \sigma^2/2$) were used to calculate $z(\theta') = 1 - R_a(\theta')/R_B$ for a set of values of σ. For this calculation, the optical constants appropriate to the long wave IR were used in the Fresnel reflectivity formula. Since an empirical relationship exists between σ and the wind speed given by Cox [1954]:

$$\sigma^2 = 0.003 + 0.00512\,w, \tag{12}$$

where w is the wind speed in m/s, this set of results is effectively parameterized by the wind speed. Figure 3 presents the calculated function $z(\theta')$ for selected values of σ. For values of θ' near 75° (15° away from grazing), modest values of the wind speed produce substantial effects. The sea can

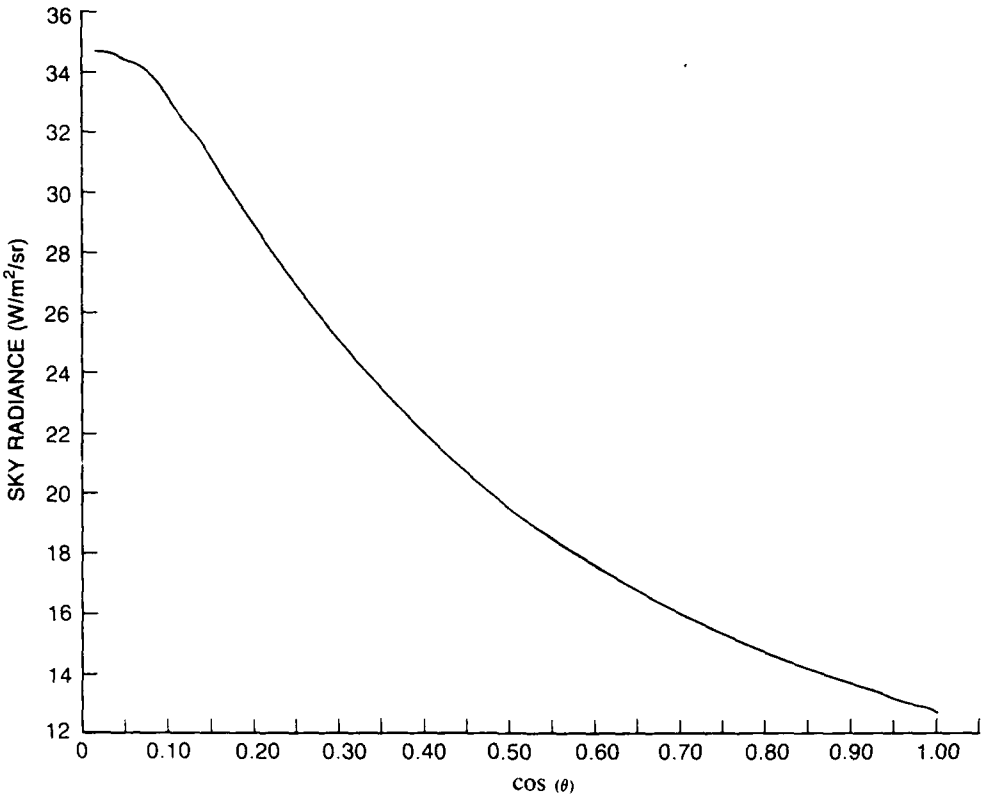

Fig. 2 — Sky radiance as a function of the cosine of the angle from the zenith

appear to emit up to 10% less radiation than a calm sea would appear to emit. Effects of this magnitude can have a substantial impact on ship detectability.

5. APPLICATION TO SHIP WAKES

When a ship moves through the water, it leaves two distinctly different wakes: Kelvin wakes and the turbulent core wake. The wake region of interest here is the surface of the turbulent core wake. One geometric feature on the sea surface that distinguishes the turbulent wake region from the background is that the surface of the wake appears to be relatively smooth. Many of the features of the background that make it rough, such as capillary waves, have been greatly reduced in the wake region. Only those waves having very long wavelengths survive. Since the width of the wake region is on the order of the length of the transom of a ship, the surface of the turbulent wake region appears as a smooth rectangular strip in a roughened sea.

In the case of the turbulent core wake, recent IR measurements show that the wake regions appear to be either cooler or warmer than the background. Daytime measurements show that the wake has an apparent temperature cooler than the apparent temperature of the surrounding rough sea [Peltzer and Garrett 1987]. Other models of the wake region have been used to compute the differences in temperature between the wake region and the background. For example, in Stewart [1987], by using a Navier-Stokes approach to the turbulent core region that includes thermal diffusion, both cooler and warmer wakes are predicted compared to the background. Cooler wakes are predicted during the day, and warmer wakes are predicted during the night. Clear sky conditions are assumed in both cases. Peltzer and Garrett [1987] and Stewart [1987] conclude that there is an intrinsic temperature difference at the sea surface between wakes and their backgrounds. Measurements were

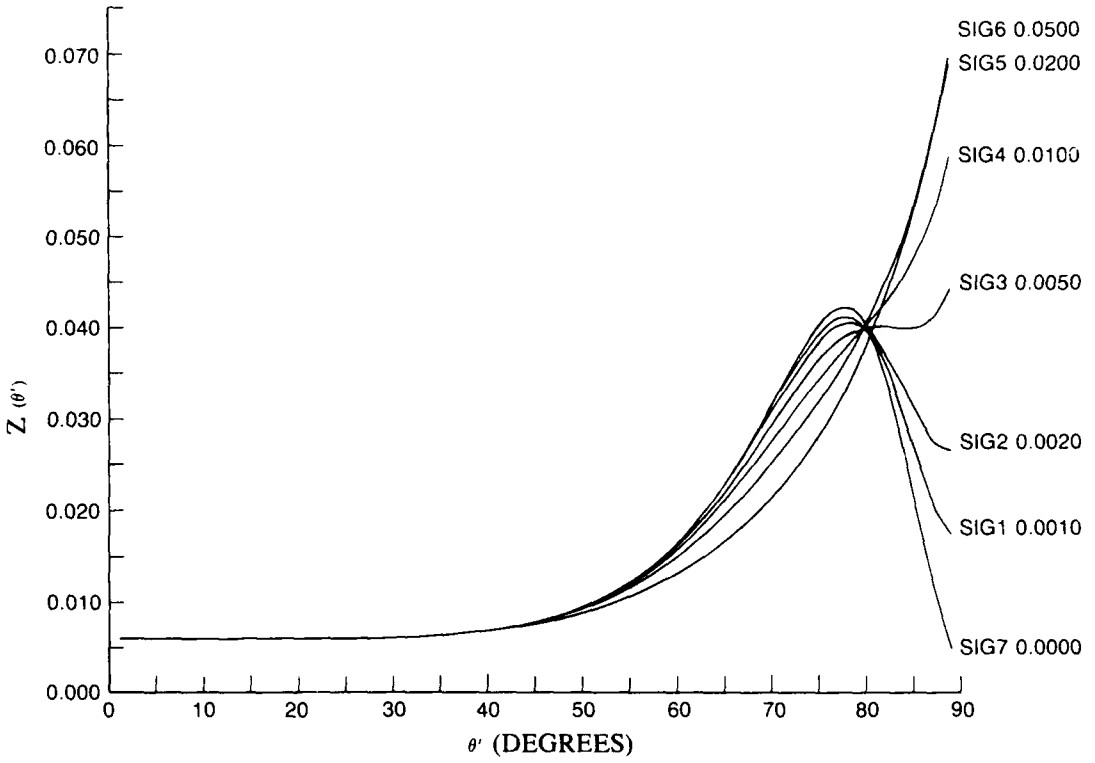

Fig. 3 — Apparent change in radiance as a function of angle.
Each curve corresponds to a value of σ.

made by Peltzer and Garrett [1987] with their sensor at near normal incidence to the wake region. Near normal incidence (the emissivity of water) is close to unity, and the reflectivity is small. As a result, measurements made at nadir consider only self-emission from the surface, while reflections from the sky off the water into the sensor are minimized. Here we argue that in the absence of a temperature difference between the wake region and its background, an apparent contrast may still be observed between the wake and its background.

By using the statistics of the facet surfaces developed in Sections 3 and 4, we compute an expected contrast between the rough surface background and the wake region. Since the surface of the wake has been smoothed in the turbulent core region, we model the surface of the wake as a flat water surface. That is, the probability density of the slope in the wake region is a delta function at the origin. Equation (5) gives the density used to compute the expected radiance of a rough sea. Expected contrast is defined to be the expected radiance of the smooth sea minus the expected radiance of a rough sea. For a fixed-view angle from the zenith, the contrast between the wake and its background is computed as a function of the background roughness, or σ, where σ is the slope variance. The slope variance varies linearly with wind speed and is given by Eq. (12). Figure 4 plots the result. The units of the contrast are $W/m^2/sr$. The sea radiance and horizon radiance used in generating Fig. 4 are equal and have a value of 34.48 $W/m^2/sr$. Results for several view angles (75°, 80°, 82°, 84°, 86°) are shown. For small values of σ and angles $\geqq 82°$, the contrast is positive and increasing. This means that the radiance of the wake region is greater than the radiance of the rough sea. As σ is increased, a maximum positive contrast is reached before the contrast decreases. Lower angles of view (such as 75° and 80°) have negative contrast values. Therefore, for viewing angles sufficiently large (i.e., near grazing), the apparent temperature of the surface in the wake region is warmer than the apparent temperature of its background. However, the intrinsic temperatures of the wake and background regions were equal.

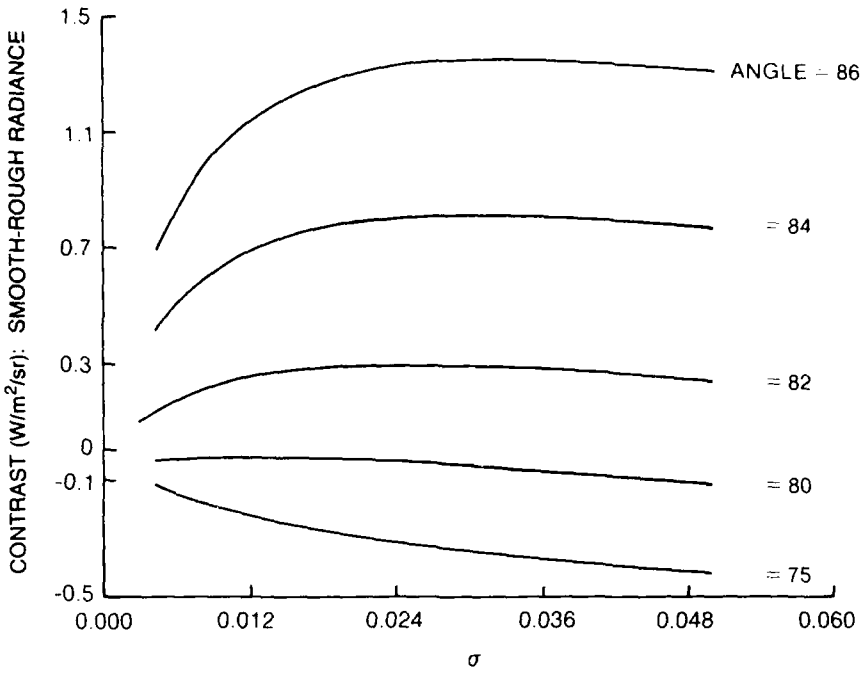

Fig. 4 — Contrast between the wake and its background as a function of σ. Each curve corresponds to a different sensor angle. The wake, sky, and background radiance values are assumed to be equal to the value of 34.48 W/m²/sr.

To analyze the major competing effects that contribute to the contrast, consider a single facet of the rough sea where the surface is flat but with unit normal located at angles (θ,ϕ). As in the previous sections, $\hat{r}$ denotes the unit vector along the LOS, and r' is the unit vector defined by Eq. (8). The spherical angles of $\hat{r}$ and r' are (respectively) $(\hat{\theta},\hat{\phi})$ and (θ',ϕ'). The reflectivity of water is denoted by $\rho(\Omega)$, where Ω is the angle defined by $n \cdot \hat{r} = \cos(\Omega)$. The slope of the surface facet is given by $\tan\theta$. The contrast radiance at view angle $(\hat{\theta},\hat{\phi})$ is the radiance of horizontal surface minus the radiance of sloped facet at (θ,ϕ) and is given by

$$C(\hat{\theta},\hat{\phi};\theta,\phi) = R_B[\rho(\Omega) - \rho(\hat{\theta})]$$

$$+ R_s(\hat{\theta})\rho(\hat{\theta}) - R_s(\theta')\rho(\Omega). \tag{13}$$

Equation (13) includes contributions from both intrinsic and reflected radiance values. The angles Ω and θ' are given as functions of $(\hat{\theta},\hat{\phi})$ and (θ,ϕ) by Eqs. (6) and (7). To highlight the effects of the reflectivity of water and the sky radiance, add and subtract the term $R_s(\hat{\theta})\rho(\Omega)$ to Eq. 13 to get

$$C(\hat{\theta},\hat{\phi};\theta,\phi) = [\rho(\hat{\theta}) - \rho(\Omega)]\,(R_s(\hat{\theta}) - R_B)$$

$$+ \rho(\Omega)\,(R_s(\hat{\theta}) - R_s(\theta')). \tag{14}$$

We now analyze the signs of the first and second terms in Eq. (14). If the angle of view is close to grazing, most of the facets seen by the sensor will be tipped up toward the sensor. Therefore, we assume for the moment that $\phi = \hat{\phi}$. Under this assumption, $\cos\Omega = \cos(\hat{\theta} - \theta)$ and

$\cos(\theta') = \cos(\hat{\theta} - 2\theta)$. If $\hat{\theta}$ and θ are in the interval $(0, \pi/2)$, then $\cos\Omega > \cos\hat{\theta}$ and $\cos(\theta') > \cos(\hat{\theta})$. (Since the slope of the sea surface is small, this inequality is reasonable for a sufficiently large $\hat{\theta}$.) Since ρ is monotone increasing, $\rho(\hat{\theta}) > \rho(\Omega)$. Note that $R(\hat{\theta}) < R_B$ for all $\theta \in (0, \pi/2)$, since the sky radiance is equal to the sea radiance at $\hat{\theta} = \pi/2$ and is monotone increasing. Therefore, the first term in Eq. (14) is negative. The second term is positive since the sky radiance is monotone increasing.

For a single facet, there are two competing effects when determining the contrast. One effect is caused by the difference between the reflectivity of flat water and the reflectivity of rough water. The second effect is caused by the difference between sky radiance reflected from flat water and that of rough water. With respect to surface roughness, the sign of the contrast, therefore, depends on the relative change between the reflectivity in the first term and the sky radiance in the second term. Before analyzing this point in detail, note that when $\phi \neq \hat{\phi}$, the angle inequalities hold when $\phi - \hat{\phi}$ is sufficiently small. Computations show, however, that the signs of the expected values of $\rho(\hat{\theta}) - \rho(\Omega)$ and $R_s(\hat{\theta}) - R_s(\theta')$ do not change if $\hat{\theta}$ is sufficiently close to grazing. (See discussion below.)

Let

$$P_\rho(\hat{\theta},\hat{\phi};\theta,\phi) = \frac{\rho(\hat{\theta}) - \rho(\Omega)}{\rho(\hat{\theta})}, \tag{15}$$

and

$$P_s(\hat{\theta},\hat{\phi};\theta,\phi) = \frac{R_s(\hat{\theta}) - R_s(\theta')}{R_s(\hat{\theta})}. \tag{16}$$

Equations (15) and (16) define the relative change in reflectivity and sky radiance as a function of facet normal at a fixed view angle $\hat{\theta},\hat{\phi}$.

We claim that then $\hat{\theta}$ is near grazing and $\phi = \hat{\phi}$, both P_ρ and P_s are increasing functions of surface roughness or slope when the facets are tipped toward the sensor. If the slope is increased, Ω is decreased. This implies that P_ρ is increasing. Likewise, increasing the slope decreases θ'. Therefore, P_s is increasing as a function of slope. When the restriction of requiring equal azimuthal angles is relaxed and the expected values of P_s and P_ρ are computed, they are both still increasing functions of σ.

By using the relative change expressions given by Eqs. (15) and (16) in Eq. (14), we find that:

$$C(\hat{\theta},\hat{\phi};\theta,\phi) = W_1(\hat{\theta},\hat{\phi};\theta,\phi)\,(R_s(\hat{\theta}) - R_B) + W_2(\hat{\theta},\hat{\phi};\theta,\phi)R_s(\hat{\theta}), \tag{17}$$

where

$$W_1(\hat{\theta},\hat{\phi};\theta,\phi) = \rho(\hat{\theta})P_\rho(\hat{\theta},\hat{\phi};\theta,\phi), \tag{18}$$

$$W_2(\hat{\theta},\hat{\phi};\theta,\phi) = \rho(\Omega)P_s(\hat{\theta},\hat{\phi};\theta,\phi). \tag{19}$$

Equation (17) explicitly shows how the contrast depends on the weights W_1 and W_2, which are proportional to P_ρ and P_s, respectively. Multiplying Eq. (17) by the density of facets seen by the sensor and integrating (θ,ϕ) over the hemisphere yields the expected contrast in terms of the expected values of W_1 and W_2 at a fixed view angle $(\hat{\theta},\hat{\phi})$. Figure 5 shows the computed results of the expected weights for several angles near grazing as a function of σ. As before, we assume that the sea radiance and the sky radiance at the horizon are equal and take values of 34.48 W/m^2/sr. The solid lines are the expected values of W_1, while the dashed lines are those of W_2. Notice that in both cases, W_1 and W_2 are increasing functions of σ. As σ is increased, W_1 has a greater rate of increase than does W_2. In particular, the ratio W_2/W_1 is on the order of 0.1 when σ is 0.05. The implication is that the reflectivity at near grazing angles of $\hat{\theta}$ changes more rapidly than sky radiance as the surface is roughened.

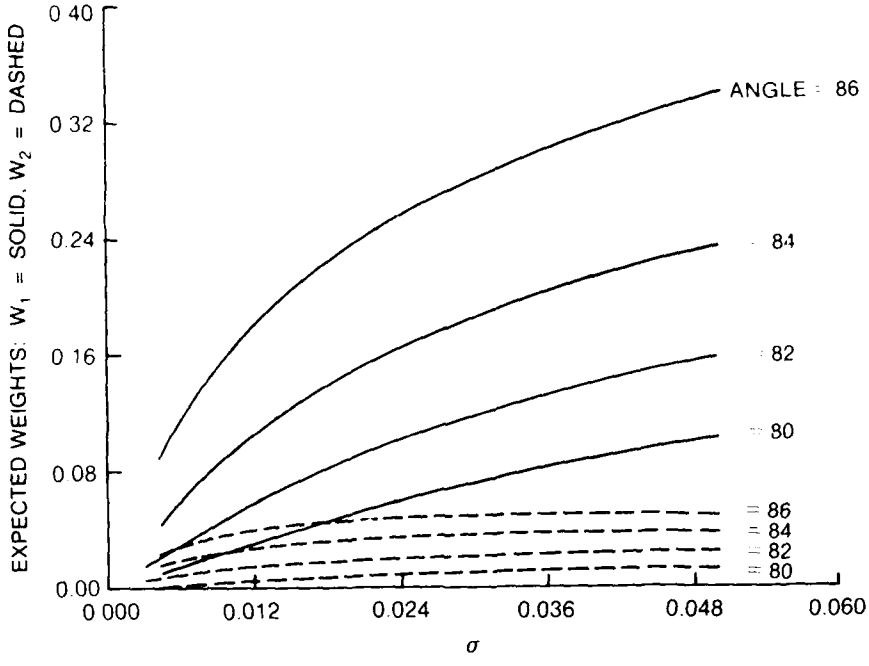

Fig. 5 — Expected values of weights W_1 and W_2 as a function of σ

Since the first term in Eq. (17) is negative, the relative change in the sky radiance needs to be greater than the change in reflectivity for the second (positive) term in Eq. (17) to become dominant. If we examine view angles near grazing, we see that the ratio W_2/W_1 needs to be small from the following argument. The expected contrast at $(\hat{\theta},\hat{\phi})$ is nonnegative if and only if

$$< W_2(\hat{\theta},\hat{\phi}) > - < W_1(\hat{\theta},\hat{\phi}) > \left[\frac{R_B - R_s(\hat{\theta})}{R_s(\hat{\theta})} \right] \geq 0, \tag{20}$$

where $< \cdot >$ denotes the expected value. Let $\hat{\theta} = \pi/2 - \epsilon$, where ϵ is small and positive. It can be shown that, to $0[\epsilon^2]$,

$$\frac{< W_2(\hat{\theta},\hat{\phi}) >}{< W_1(\hat{\theta},\hat{\phi}) >} \geq \frac{\epsilon \dfrac{dR_s\ (\pi/2)}{d\theta}}{R_s\ (\pi/2 - \epsilon)}. \tag{21}$$

Since the sky radiance changes slowly near the horizon, the derivative of R_s is small (less than unity), while the value of R_s near the horizon is an order of magnitude greater. Therefore, for small positive contrast values, $< W_2 >$ must be on the order of $0.1\epsilon < W_1 >$. That is, the sky radiance changes more slowly than the reflectivity at near grazing angles.

Note that when $\hat{\theta}$ is not near grazing, either one or both of the expected weights may be negative, as a function of σ. For example, in Fig. 4, the contrast is negative when $\hat{\theta} = 75°$. In this case $< W_1 >$ is positive and increasing, while $< W_2 >$ is negative.

This discussion shows that a nonzero contrast between a wake and its background can be driven by pure reflection instead of an intrinsic temperature difference between the wake and its background. We now consider wake temperatures that are cooler than background, which means that wake blackbody radiance is lower than background blackbody radiance. The radiance in the wake region is decreased by an amount equal to the difference between wake and background regions reported in Peltzer and Garrett [1987]. The sky radiance at the horizon and rough sea radiance were assigned the same value of 34.48, as before. We perform the same computations as in Fig. 4 and compute the contrast between the wake and its background. Figures 6 and 7 show the results. In Fig. 6 the radiance in the wake region is 33.93, and in Fig. 7 the radiance in the wake region is 32.85. Notice that in both Figs. 6 and 7 the overall contrast is reduced. Angles such as 82° no longer have a positive contrast for all values of σ. (Compare Figs. 4 and 6.) Figure 7 shows that angles greater than 86° exhibit positive contrast only if σ is large enough. Nevertheless, given an intrinsic temperature difference where the wake is cooler than its background, we conclude that it is still possible to have an apparently warmer wake than its background when viewed near grazing.

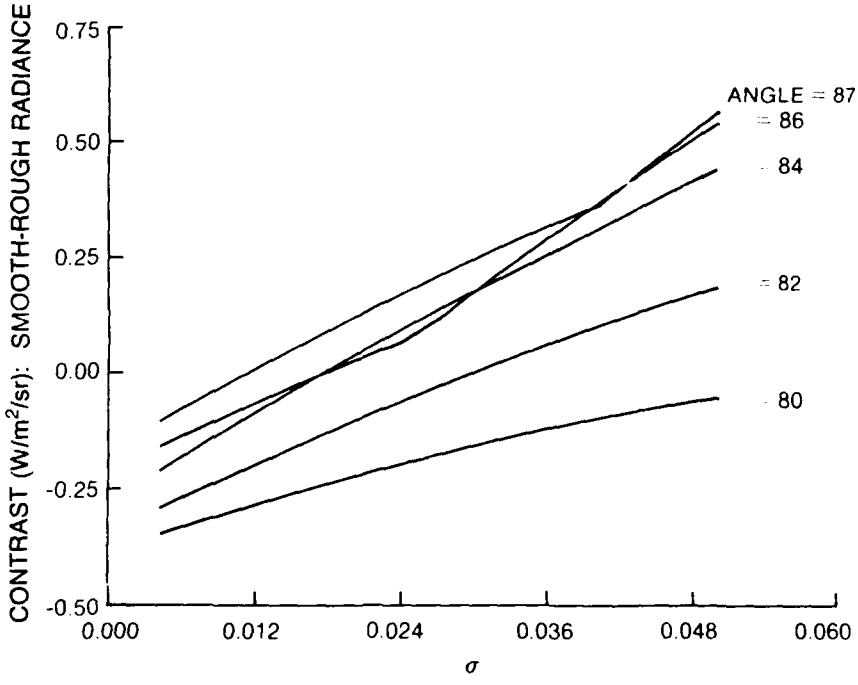

Fig. 6 — Contrast between the wake and its background as a function of σ. Same as in Fig. 4, but the wake radiance is cooler than the background radiance. The sky and background radiance values are equal to 34.48 W/m²/sr. The wake radiance is equal to 33.93 W/m²/sr.

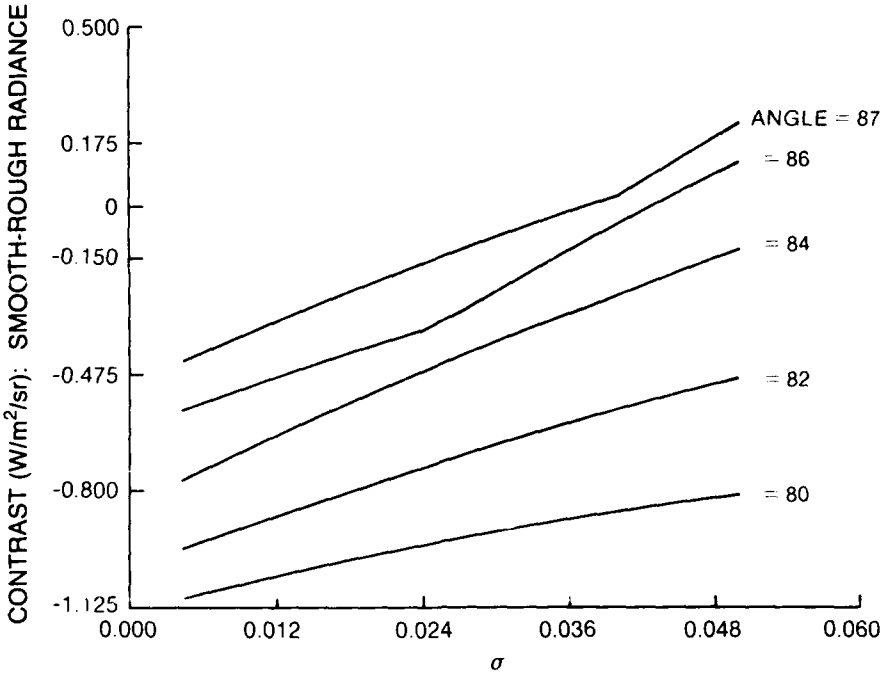

Fig. 7 — Contrast between the wake and its background as a function of σ. Same as Fig. 6, but the value of the wake radiance is less than the value used in Fig. 6. Here the wake radiance is 32.28 W/m²/sr.

6. DISCUSSION

We have presented a model of the contrast between a ship's wake and its background. Modeling of the background entailed the use of a probabilistic model of a rough sea, while the ship's wake was modeled as a smooth surface. We conclude that in the absence of an intrinsic temperature difference between the wake and its background, the apparent temperature of the wake could still appear to be warmer than its background. We observe that a rough sea can emit a substantially lower amount of radiation in the infrared when compared to a smooth sea surface. The sea, being a poor emitter of radiation at near grazing angles, reflects cool sky radiation from higher points in the sky. It therefore looks colder than its blackbody temperature. When considering near grazing angles of view, the smooth wake reflects radiation from the sky at a lower angle, and therefore, the reflected sky radiation off the wake is warmer than reflected sky radiation off the rough sea background. The reflectivity (and emissivity) of the surface also affects the contrast. The details of how the sky radiance and reflectivity of the surface affect the contrast were analyzed in Section 5, where change in reflectivity is compared to the change in sky radiance as σ is increased.

Although real temperature differences between wake and background were reported in Peltzer and Garrett [1987] and Stewart [1987] where the wake was cooler than its background, the wake can still appear to be warmer than its background, as described in Section 5. However, the roughness of the surface (σ) must be increased and/or the angle of view must be closer to the horizon. Increasing the surface roughness decreases the reflected radiation from the rough sea; increasing the view angle increases the reflected radiation from the smooth sea. Clearly, if the sea is sufficiently cool, there are no angles for which the contrast is positive.

Other authors have modeled the rough surface phenomenon as well but without the aid of a probability model of the sea slopes [Borrego and Machado 1985 and Wilf and Manor 1984]. In some extreme cases, other authors rely on one emissivity value of the sea surface for all angles [Singh and Warren 1983].

Another popular but realistic method of computing the apparent radiance of a rough sea is to create a surface that has the same amplitudes of its Fourier components as a rough sea. The method is called the power spectral approach, and it has been used either directly or indirectly in simulating images of a rough sea [Menat 1976, Schwartz and Hon 1986 (for a description of the technique), Chapman and Irani 1981, Ben-Yosef et al. 1983, Borrego and Machado 1985, Sidran 1981, Wilf and Manor 1984]. The power spectral method is computationally intensive since a large number of facets must be considered. Furthermore, many surfaces must be generated to compute statistical information about the sea surface in question for each wind speed. Analyzing the power spectral model is difficult. Our probabilistic approach, however, immediately generates the statistics of the rough sea surface with a minimum amount of computational effort. The physics is contained in the model at a glance, thus making it easy to analyze and verify in certain cases.

Finally, our slope magnitude model of the sea surface is a two-dimensional model based on linear superposition of waves. Real sea surfaces, however, have nonlinear waves, as pointed out in Huang et al. [1983,1984]. In particular, Huang et al. have derived the probability slope distribution for a nonlinear wave in one dimension. In Huang et al. [1984], a small parameter σk is introduced where σ is the standard deviation of the surface elevation and k is the wave number. By using the assumption that the parameter is small, the probability slope density can be shown to be normal to order $(\sigma k)^2$. However, small changes in wave slopes can possibly lead to substantial changes in reflected radiation. Therefore, nonlinear waves may, in fact, affect the contrast when viewed near grazing.

REFERENCES

P. Beckmann and A. Spizzichino, *The Scattering of Electromagnetic Waves from Rough Surfaces* (Pergamon, New York, 1963).

N. Ben-Yosef, B. Rahat, and G. Feigin, "Simulation of IR Images of Natural Backgrounds," *Appl. Opt.* **22**, 190 (1983).

J.A. Borrego and M.A. Machado, "Optical Analysis of a Simulated Image of the Sea Surface," *Appl. Opt.* **24**, 1064 (1985).

R.D. Chapman and G.B. Irani, "Errors in Estimating Slope Spectra from Wave Images," *Appl. Opt.* **20**, 3645 (1981).

C. Cox and W. Munk, "Measurement and Roughness of the Sea Surface from Photographs of the Sun's Glitter," *J. Opt. Soc. Am.* **44**, 838 (1954).

J.B. Goodell, "The Appearance of Sea Reflected Sky," *Appl. Opt.* **10**, 223 (1971).

N.E. Huang, S.R. Long, C.C. Tung, Y. Yuen, and L.F. Bliven, "A Non-Gaussian Statistical Model for Surface Elevation of Nonlinear Random Wave Fields," *J. Geo. Phys. Res.* **88**, 7597 (1983).

N.E. Huang, S.R. Long, L.F. Bliven, and C.C. Tung, "The Non-Gaussian Joint Probability Density Function of Slope and Elevation for a Nonlinear Gravity Wave Field," *J. Geo. Phys. Res.* **89**, 1961 (1984).

P. Lecompte, P.Y. Deschamps, and J.C. Vanhoutte, "Ameliorations apportees a la mesure de la temperature de surface de l'ocean par l'utilisation d'un radiometre infrarouge polarisant," *Appl. Opt.* **12**, 2115 (1973).

J.R. Maxwell, J. Beard, J. Weiner, D. Ladd, and S. Ladd, "Bidirectional Reflectance Model Validation and Utilization," Air Force Avionics Laboratory Report AFAL-TR-73-303, Oct. 1973.

M. Menat, "Infrared Contrasts in Reflecting-Sea Surroundings," *Infrared Phys.* **16**, 577 (1976).

R.D. Peltzer and W.D. Garrett, "A Remote Sensing Study of a Surface Ship Wake," *Int. J. Remote Sensing* **8**, 689 (1987).

I.B. Schwartz and D. Hon, "Emissivity as a Function of Surface Roughness: A Computer Model," NRL Memorandum Report 5816, August 1986.

M. Sidran, "Broadband Reflectance and Emissivity of Specular and Rough Water Surfaces," *Appl. Opt.* **20**, 3176 (1981).

S.M. Singh and D.E. Warren "Sea Surface Temperatures from Infrared Measurements" in Remote Sensing Applications in Marine Science and Technology, A.P. Cracknell, ed. (Plenum Press, New York, 1983) p. 231.

B.G. Smith, "Geometrical Shadowing of a Random Rough Surface," *IEEE Trans. Antennas Propag.* **AP-15**, 668 (1967).

M. Stewart, "Numerical Prediction of Thermal Ship Wakes," NRL Memorandum Report 5955, Sept. 1987.

K.E. Torrence and E.M. Sparrow, "Theory for Off-Specular Reflection from Roughened Surfaces," *J. Opt. Soc. Am.* **57**, 1105 (1967).

I. Wilf and Y. Manor, "Simulation of Sea Surface Images in the Infrared," *Appl. Opt.* **23**, 3174 (1984).

Appendix A

DERIVATION OF SLOPE PROBABILITY DENSITY

We begin by considering the function $z = h(x,y)$ defined to be the water height above mean sea level at the position (x,y) in the horizontal plane. The function h may be regarded to be a random function, that is, $h(x,y)$ is to be regarded as a random variable for each value of x and y. Corresponding to this type of random variable is a probability density function. Because the surface of the ocean is translationally invariant in a statistical sense, the density does not depend on x and y. Accordingly, we denote it by p. The value of $h(x,y)$ is the sum of contributions from waves of a large range of wavelengths. To the extent that the contributions of the different wavelengths are statistically independent, the central limit theorem applies and p is of normal form. This assumption of independent contributions is an approximation that breaks down for large values of h as the result of nonlinear hydrodynamic interactions. However, it is a good approximation for our purposes here. The wave slope is the gradient of h. The statistics of spatial derivatives can be calculated by the use of finite differences, namely:

$$\frac{\partial h}{\partial x} \simeq \frac{h(x',y)\, h(x,y)}{x'y} \tag{A1}$$

for x' sufficiently close to x. (A similar relation holds for $\partial h/\partial y$.) It is established that wavelengths shorter than a certain cutoff contribute little to the slope statistics. Consequently, Eq. (A1) may be considered valid as long as $| x' - x |$ is less than the cutoff length. If the anisotropy introduced by the wind direction is ignored, $h(x',y)$ and $h(x,y)$ are identically normally distributed random variables. They are correlated with a correlation length depending on $| x' - x |$. Since the difference of two correlated normally distributed random variables is itself a normally distributed random variable, it follows that $\partial h/\partial x$ and $\partial h/\partial y$ are normally distributed. The wave slope s is defined to be the magnitude of the gradient of h, i.e.,

$$s = \sqrt{\left(\frac{\partial h}{\partial x}\right)^2 + \left(\frac{\partial h}{\partial y}\right)^2}. \tag{A2}$$

Since $\partial h/\partial x$ and $\partial h/\partial y$ are normal, independent with zero mean and equal variance, the random variable s has a Rayleigh density, given by

$$p_s(s) \propto s e^{-s^2/\sigma^2}, \tag{A3}$$

where $\sigma 2$ is the slope variance. It is more convenient to work with a description in terms of spherical coordinates on a unit sphere. We introduce the angle coordinates θ,ϕ to describe the direction of the unit normal n to the facet face. The angle θ is the angle between n and the normal-to-the-sea surface (the z direction), while ϕ is the azimuthal angle defined as 0 when n is in the z,x plane. Because $s = \tan\theta$, it follows from a change of variables that

$$p_n(\theta,\phi) = (1/2\pi)2\sigma^2 \tan\theta \sec^2\theta\, e^{-\tan 2\theta/\sigma^2}. \tag{A4}$$

It is easy to see how the nonisotropic case in which the upwind and crosswind variances are unequal generalizes the probability slope distribution. Assume that the x and y directions correspond to the upwind and crosswind directions, respectively, and also suppose that the mean slopes are zero in both x and y directions. A normal vector to the surface at (x,y) is given by

$$N(x,y) = (\partial\Phi/\partial x, \partial\Phi/\partial y, 1) = [s^2 + 1]^{1/2}\, n(x,y). \tag{A5}$$

Decomposing the vector $N(x,y)$ into spherical coordinates (θ,ϕ) on the sphere of radius $[s^2 + 1]^{1/2}$, it follows that $\sin\theta = s/[s^2 + 1]^{1/2}$ and $\tan\theta = s$.

Reasoning as before, the slope density $p(\partial h/\partial x, \partial h/\partial y)$ is normal in both arguments with standard deviations σ, σ and correlation coefficient r. We make the change variables by letting

$$\partial\Phi/\partial x = \sqrt{s^2 + 1}\,\sin\theta\cos\phi = \tan\theta\cos\phi,$$

$$\partial\Phi/\partial y = \sqrt{s^2 + 1}\,\sin\theta\sin\phi = \tan\theta\sin\phi. \tag{A6}$$

Since the Jacobian of the transformation is $\sec 2\theta \tan\theta$, the new density in terms of (θ,ϕ) is given by

$$\hat{p}_n(\theta,\phi) = \frac{\sec 2\theta \tan\theta}{2\pi\sigma_x\sigma_y\sqrt{(1 - r^2)}} \exp\left\{\frac{\tan 2\theta}{2(1 - r^2)} E(\phi,r)\right\}, \tag{A7}$$

where

$$E(\phi,r) = \frac{\cos 2\phi}{\sigma_x^2} + \frac{\sin 2\phi}{\sigma_y^2} \quad \frac{2r\cos\phi\sin\phi}{\sigma_x\sigma_y}, \tag{A8}$$

and n is $N/\|N\|$. Notice that if $\sigma = \sigma$ and $r = 0$, then the probability density is given in terms of θ only and reduces to Eq. (A4).